esteem3

Enabling Science through European Electron Microscopy

First report on TEM methods applied to ICT materials

Deliverable D7.1 – version 1

Estimated delivery date:	M16 April 2020
Actual delivery date:	June 8th, 2020
Lead beneficiary:	GRA, ZAR
Person responsible:	Gerald Kothleitner, Raul Arenal
Deliverable type:	☒ R ☐ DEM ☐ DEC ☐ OTHER ☐ ETHICS ☐ ORDP
Dissemination level:	☒ PU ☐ CO ☐ EU-RES ☐ EU-CON ☐ EU-SEC

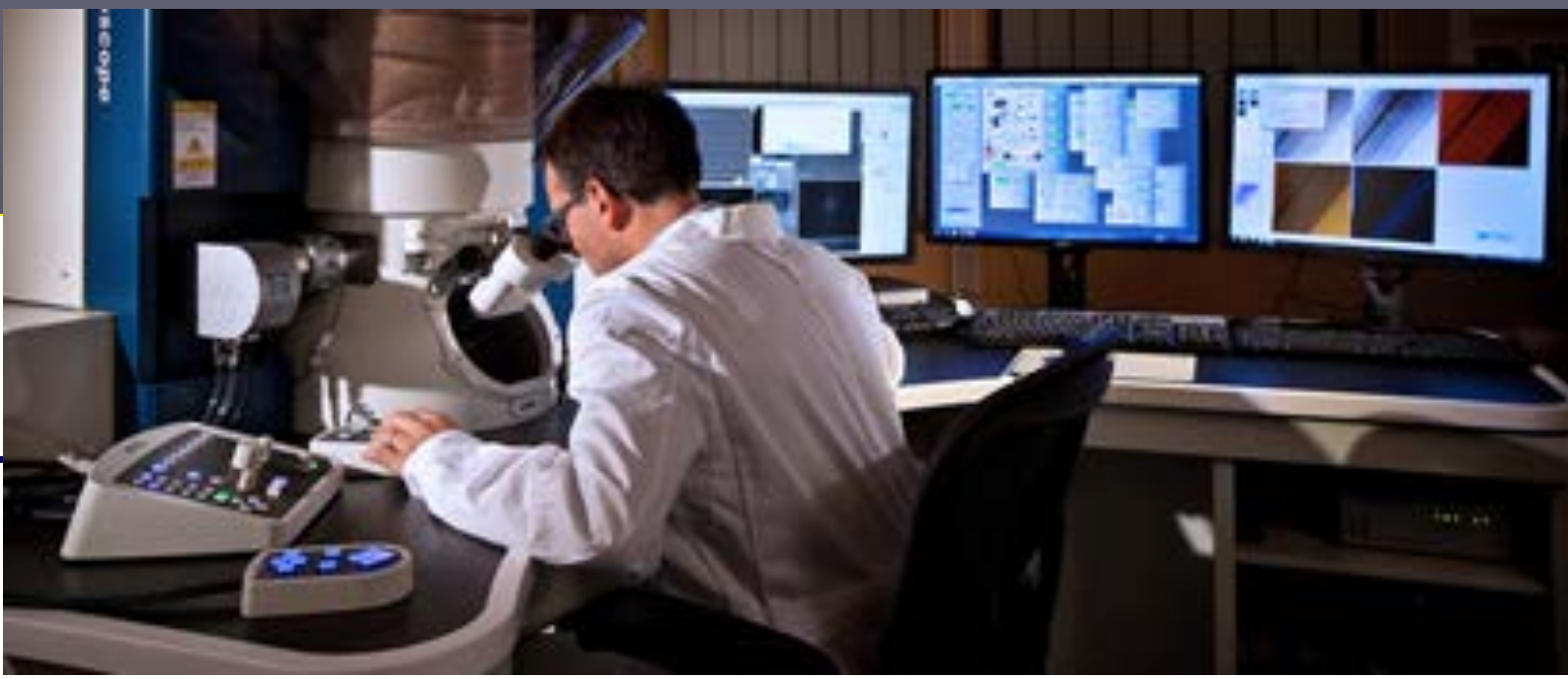

THIS PROJECT HAS RECEIVED FUNDING FROM THE EUROPEAN UNION'S HORIZON 2020 RESEARCH AND INNOVATION PROGRAMME UNDER GRANT AGREEMENT NO **823717**

Grant Agreement No:	823802
Funding Instrument:	Research and Innovation Actions (RIA)
Funded under:	H2020-INFRAIA-2018-1: Integrating Activities for Advanced Communities
Starting date:	01.01.2019
Duration:	48 months

Table of contents

Revision history log

Version number	Date of release	Author	Summary of changes
V0.1	30.04.2020	Gerald Kothleitner	Preparation of the initial version of the report.
V0.2	15.05.2020	Raul Arenal	Corrections & additions (text & figures).
V0.3	20.05.2020	Gerald Kothleitner	Further minor corrections requested by partners.
V0.4	02.06.2020	Eva Olsson	Changes to fig. 6
V1.0	06.06.2020	Gerald Kothleitner	Finalization
V1.1	08.06.2020	Lucie Guilloteau	General review of the deliverable
V.1.2	08.06.2020	Peter A. van Aken	Final check and validation

Introduction

The functionality and availability of future generations of Information and Communications Technologies (ICT), critically depend on the discovery, exploration and understanding of the fundamental physico-chemical principles that underlie the various electronic / magnetic / photonic / semiconducting materials used in the ICT industry. The large diversity of required functionalities and the broad range of materials needed, require powerful characterization techniques, ranging from specimen preparation to diffraction and imaging, electron tomography, spectroscopy, holography and in-situ investigations, with adequate energy and spatial resolution. The work package explores the applicability of TEM in the context of the pertinent physical phenomena and its best use with respect to a certain class of materials. Formally the work is split into four tasks, however, intrinsic to the nature of the materials, some of the results presented within a task, occasionally overlap with other tasks and work packages. This deliverable shall emphasize some of the key findings within the first 18 months of the project, and highlights the strengths of (the combination of) techniques used so far. Methods, techniques, findings which were most relevant to the investigations on the respective ICT material are formatted in bold letters.

Task 7.1: Semiconducting and magnetic materials (GRA, ZAR, CHA, TOU*, CAT*)

Focused Electron Beam Induced Deposition (FEBID), having become a mature nanofabrication technique, was explored to enable highly localized synthesis of functional nanostructures. This direct-writing nanofabrication method has proven to be unique for the development of 2D and 3D objects with spatial resolution in the range of nanometers, without the need of masks, resists, etching- or lift-off processes. The decomposition of a precursor gas adsorbed on the substrate surface by an accurately-directed electron beam, enables the deposition of **metallic, magnetic, insulating and superconducting** materials only in the areas scanned by the beam. It thereby opens up a broad spectrum of applications, covering circuit edit and mask repair, micro- and nano-contacting, photodetection, nano-sensing, magneto-mechanical actuation systems or plasmonics. One of FEBID's main issues is the existence of chemical impurities due to incompletely-dissociated precursor molecules leading to incorporation of unwanted fragments inside the deposit (often containing C and O), compromising the desired functionality. Two examples shall be given on the purification and quality of **magnetic FEBID nanorods**.

Ultrathin 3D ferromagnetic **Fe nanowires** (<50 nm) fabricated by FEBID with a $Fe_2(CO)_9$ precursor have been deposited to study the morphological, compositional and crystallinity changes as a function of temperature and time, to enable applications for instance in magnetic force microscopy (MFM) magnetic sensing and catalysis. [1]

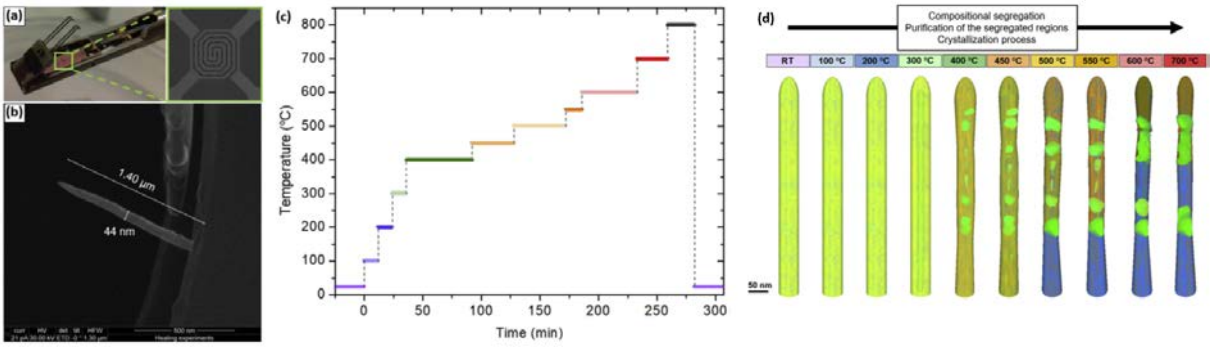

Figure: 1 Heating chip mounted in the TEM holder with (b) an Fe-FEBID nanowire grown for real-time TEM annealing experiments. (c) Temperature profiles for the Fe-FEBID. (d) Sketch of the morphology, dimensions and composition distribution of an Fe-FEBID NW as a function of the annealing temperature as observed in the experiments. Fe, O and C are depicted in green, red and blue, respectively. [from 1]

The morphological, compositional and crystallinity changes as a function of the temperature and time have been monitored in real time inside a transmission electron microscope with **2D dark-field STEM imaging** and **3D analytical EELS tomography** (figure 1).

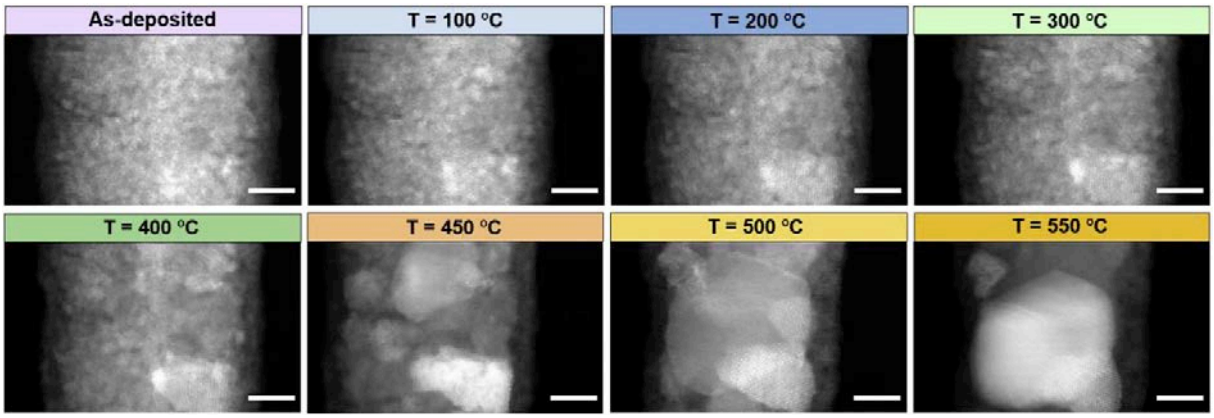

Figure: 2 In-situ annealing experiments and observation of structural evolution to obtain magnetic functionality. [from 1]

According to the obtained results, annealing up to 700 °C of an as-grown homogeneous nanocrystalline nanowire with an initial metallic content of about 40 at. % Fe induces the coexistence of Fe-purified and crystallized regions in the nanowire with other Fe-deficient amorphous regions (figure 2). Thus, instead of the full metal purification, a strong phase segregation in the nanowire is provoked. **The work underlines the importance of in-situ studies with nanoscale resolution for the optimization of nanomaterials, and the understanding of their functionality** not in terms of their average physical properties, but of the physical properties of their individual constituents.

For **MFM imaging** a big advantage of these tips, in comparison with CoCr coated pyramidal probes, lies in the capability of creating sharp ends, nearly 10 nm in diameter, which **provides remarkable (topographic and magnetic) lateral resolution** in samples with magnetic features close to the resolution limits of the MFM technique itself (figure 3). [2]

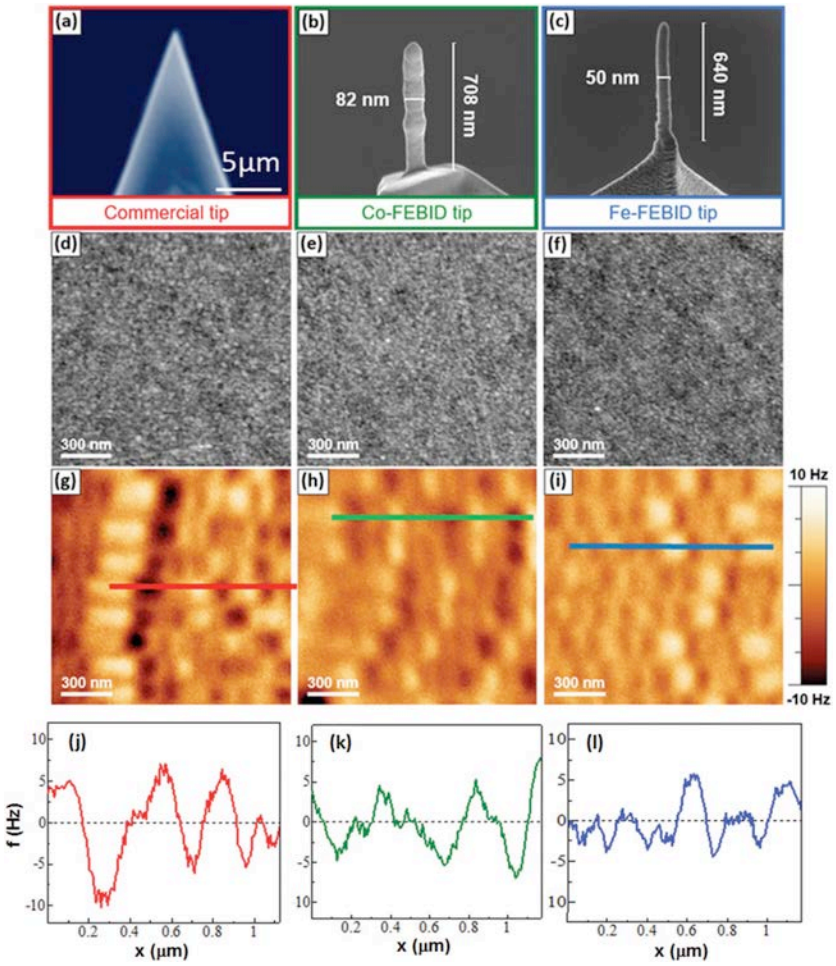

Figure 3: Images of (a) Commercial Budget Sensors MFM tip with 50 nm of CoCr coating, (b) Co-based FEBID tip and (c) Fe-based FEBID tip grown on Nanoworld Arrow EFM cantilevers. (d, e, f) Topographic images of a hard disk reference sample obtained by the selected MFM probes and (g, h, i) their corresponding magnetic images and profiles (j, k, l), respectively. Z lift was 30 nm in all cases. [from 2]

The shape of the **nanorods produces a very confined magnetic stray field, whose interaction with the sample is extremely localized and perpendicular to the surface, with negligible in-plane components** (figure 4). Besides, the high-aspect ratio achievable in FEBID nanorod tips makes them **magnetically harder** than the commercial ones, reaching **coercive fields higher than 900 Oe**, which is a highly desirable feature for MFM measurements in in situ applied field experiments.

Fig. 4 (a) STEM-EELS chemical profile of an Fe-based nanorod grown on top of an AFM probe. The vertical short dash-dot line represents the nanorod apex edge. The top inset is a chemical map showing the relative composition of Fe, C and O contents in green, blue and red, respectively. The bottom inset is the corresponding TEM image. (b) Cosine color map: composite image displaying the magnetic field inside and outside the tip using a colour scale for the direction and intensity of the integrated magnetic induction composed of the phase signal (black lines) displayed with a cosine for highlighting the magnetic flux. (c) Quantitative decay of the magnetic induction component parallel to the nanorod axis as a function of the distance from the apex determined directly from the magnetic phase image in (b) (dashed blue line), and using the Abel transform (bold red line). [from 2]

Magnetic, structural and chemical changes have also been performed on **cylindrical, textured, Co-rich CoNi nanowires**. Prepared by electrodeposition into self-assembles pores of anodic aluminum oxide templates, they displayed grains of both face-centered cu-bic (fcc) and hexagonal close packed (hcp) crystal structures, with grain boundaries parallel to the nanowire axis direction. **Electron holography and micromagnetic simulations** evidenced the existence of a complex exotic magnetic configuration characterized by two distinctly different types of magnetic configurations within a single nanowire: **an array of periodical vortices** separating small transverse domains in hcp rich regions with perpendicular easy axis orientation, and a mostly **axial configuration parallel** to the nanowire axis in regions with fcc grains. These vastly different domains are found to be caused by local variations in the chemical composition (**determined by EELS**) modifying the crystalline orientation and/or structure, which give rise to change in magnetic anisotropies. [3]

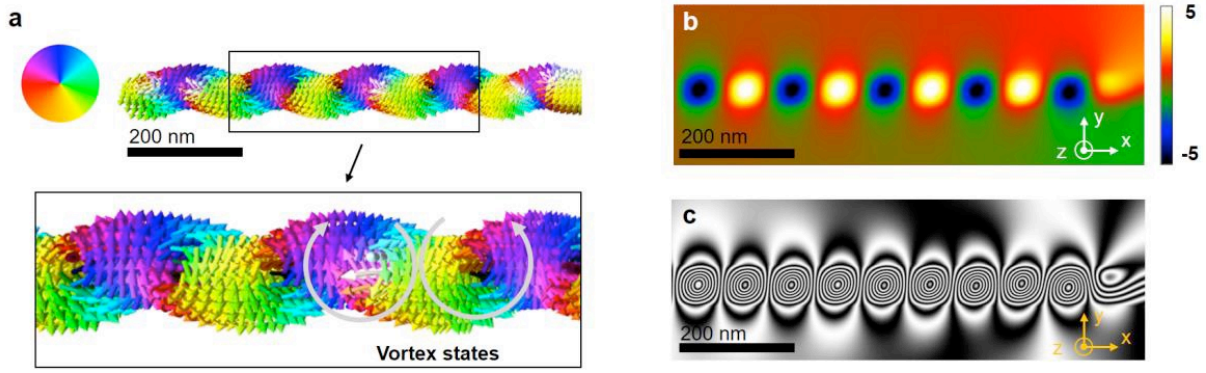

Fig. 5 Results from micromagnetic simulation. (a) 3D representation of the simulation showing the magnetic vectors with their x-y-direction indicated by the color wheel. Zoomed images of the vortex state displayed below in (a). (b) Magnetic phase image and (c) magnetic flux lines obtained from the simulation. [from 3]

Linked to **novel deposition and structuring routes**, beam induced effects not only play an important role for FEBID deposition and but also during investigations. On clustered Ni0.3Au0.7 alloy consisting of a few hundred atoms, strong segregation above the miscibility gap (>400°C) was observed already at rather low doses. These effects could be attributed to displacements of cluster atoms by elastic scattering with incident electrons. The exponential temperature relationship of the **segregation kinetics**, was explained by beam-induced displacement events followed by diffusive relaxation processes – an effect that needs to be considered particularly for non-equilibrated structures. [4]

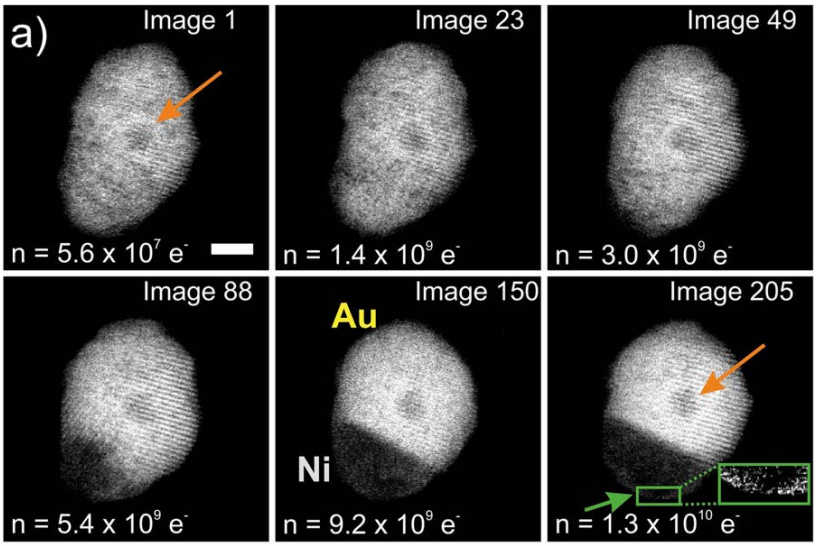

FIG. 5. (a) ***STEM HAADF image*** *series showing the beam-induced phase separation of an initially alloyed Ni-Au cluster at 600 °C; orange arrows mark the stable Ni rich inclusion in the Au phase. The green arrow in the last image marks a stable Au layer on the Ni surface; the inset shows an enlarged image of the region. [from 4]*

Semiconductor III-V nanowires and -tips have also been investigated in the context of **charge transport properties** as for p-doped GaAs nanowires, which are promising components for nanoscale optical and electronic devices (solar cells, photodetectors, logic transistors). Those applications originate from their unique band structure characteristics, such as a direct band gap with the energy within the visible light interval, small effective electron mass, and high charge carrier mobility. The **band structure** of GaAs nanowires shows sensitive response to mechanical strain, which was investigated by a combination of in-situ bending tests and EELS measurements – a collaboration with Microsoft. [5]

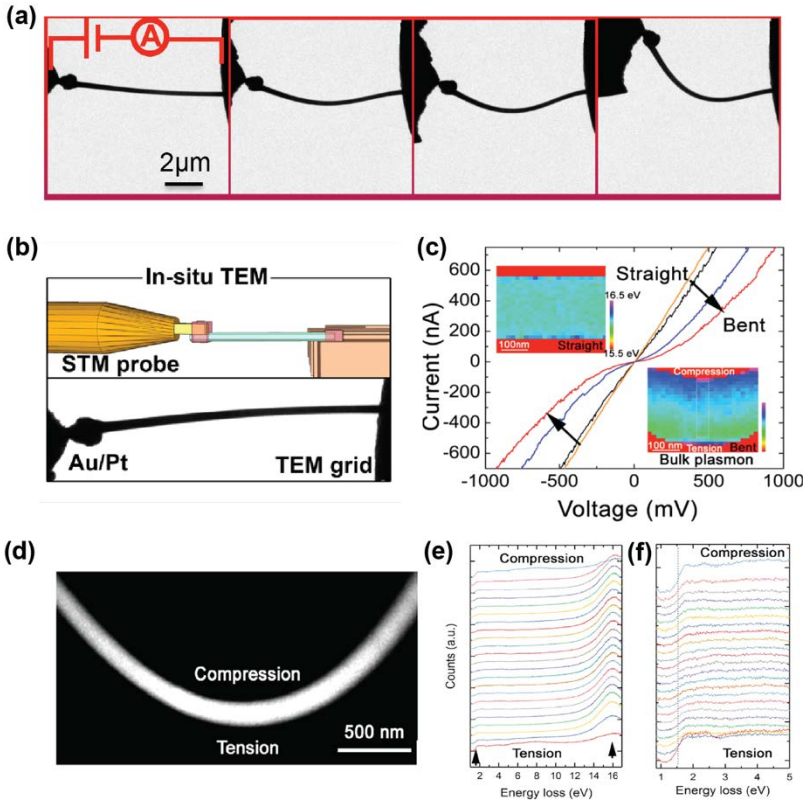

Fig. 6 The effect of bending deformation on I–V characteristics of single GaAs nanowires. (a) A series of TEM images showing the gradual bending of the nanowire by a scanning tunneling microscope (STM) probe in an in situ STM-TEM setup. The STM-TEM setup is used to simultaneously apply stress and measure I-V characteristics of single GaAs nanowires. (b) Top: A schematic of the in situ STM-TEM setup. Bottom: A TEM image showing the STM probe, the nanowire and the TEM grid used as the support for the nanowire inside TEM. (c) I-V curves of the nanowire under different levels of bending strain. Inset: bulk plasmon energy maps of the nanowire with and without bending deformation, measured using EELS. (d) A STEM HAADF image showing the bent region of the nanowire. (e) and (f) Valence EEL spectra showing the evolution in bulk plasmon energy and band gap in the bent region of the nanowire. [from 5]

The increasing nonlinearity in the I‑V characteristics with strain (figure 6) indicated the development of an energy barrier for charge carriers along the nanowire length direction due to the bending deformation. This was further investigated by **in-situ STEM-EELS** measurements and **simulations**. It could be shown that the bending deformation does not give rise to a change in the band gap; instead, the response to bending deformation could be explained by a strain induced valence band shift, producing an energy barrier for charge carriers along the nanowire, which results in the **observed change in electrical transport characteristics** (figure 7).

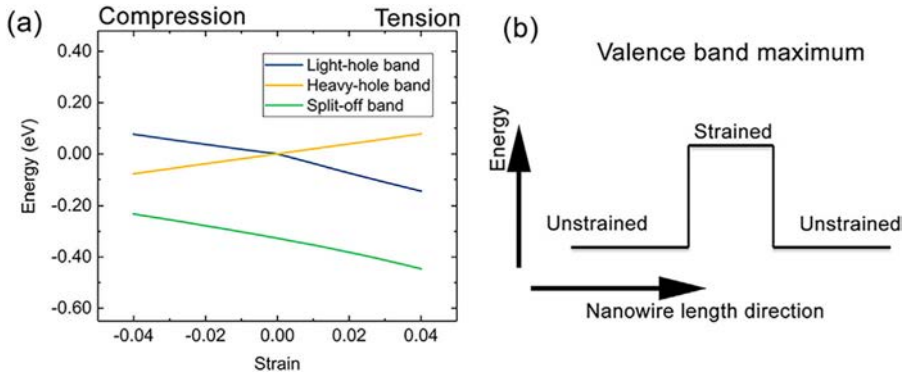

Figure 7. Shift of the valence bands due to strain: a) sp^3-d^5 tight-binding simulation of the shift of the valence band top in GaAs nanowire due to strain. b) The shift of the valence band maximum in the bent region can create an energy barrier for hole transport along the p-doped nanowire. [from 5]

Task 7.2: Functional complex oxides, carbon and related nanostructures (ZAR, STU, ORS, TOU*)

Complex Oxide Thin Films (functional complex oxide heterostructures and multilayers), particularly those with perovskite structure, that - within the same basic crystal structure - exhibit a wealth of physical phenomena: magnetism, ferroelectricity, piezoelectricity, and superconductivity upon small lattice distortions induced by chemical variations. Some of these properties, absent in bulk form, are exclusive to thin film specimens, in which epitaxial strain and the formation of interfaces induces novel phenomena such as multiferroicity (scarce in bulk), interfacial 2D electron gases or domain wall conductivity and magnetism. The grand challenges in this task lay for instance on the accurate determination of atomic columns within a structure (cations and oxygen anions) and at interfaces, which is the key to translate obtained image contrasts into maps of physical properties.

For instance, the perovskite La:$BaSnO_3$ has gained interest as a novel transparent conducting oxide (TCO) due to its high mobility at room temperature for applications in electronic devices such as transparent displays and transistors. This high mobility has been attributed to the small electron-phonon interaction and small electron effective mass arising from the large dispersion of the conduction band composed of Sn 5s orbitals. Nevertheless, by going from bulk to epitaxial thin films, a **reduced electron mobility** is encountered that is related to the formation of **dislocations**, which form upon lattice mismatches between film and substrate. [6]

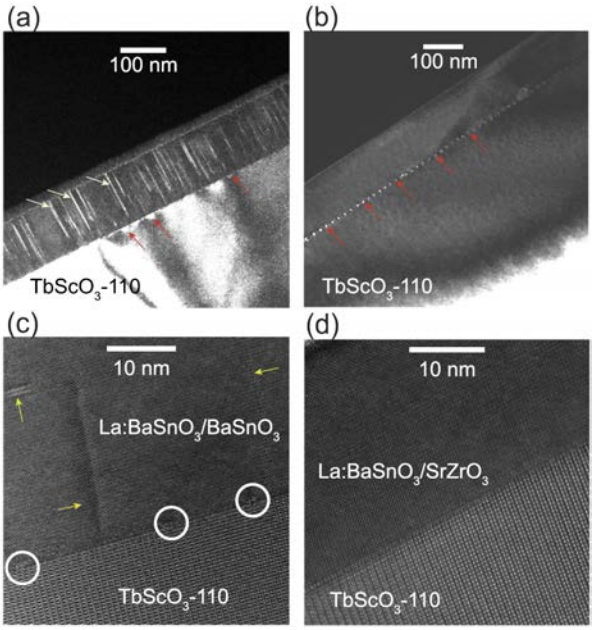

Figure 7. Weak-beam dark-field TEM images (a,b) and high-resolution TEM images (c,d) from La:$BnSnO_3$ in combination with different buffer layers ($BaSnO_3$ and $SrZrO_3$) on top of a substrate. from [6]

Weak-beam dark-field TEM images (figure 7) nicely reveal misfit dislocations along the interfaces (shown by red arrows). Specifically, edge-type threading dislocations are visible in (a), indicated by vertical bright contrasts (white arrows), and only periodic misfit dislocations are visible in (b). **High-resolution aberration-corrected TEM** images for the same heterostructures show misfit dislocations indicated (white circles in (c)) and suggest a fully relaxed interface. Stacking faults (yellow arrows) are also visible. An almost fully strained interface is seen in (d) with no apparent structural defects. In the $SrZrO_3$ buffered sample, double the mobility has been achieved in comparison to the unbuffered sample, grace to a significant reduction in the dislocation density. **This example demonstrates how the right combination of TEM imaging methods can be meaningfully linked to relevant technological parameters in such electronic devices.**

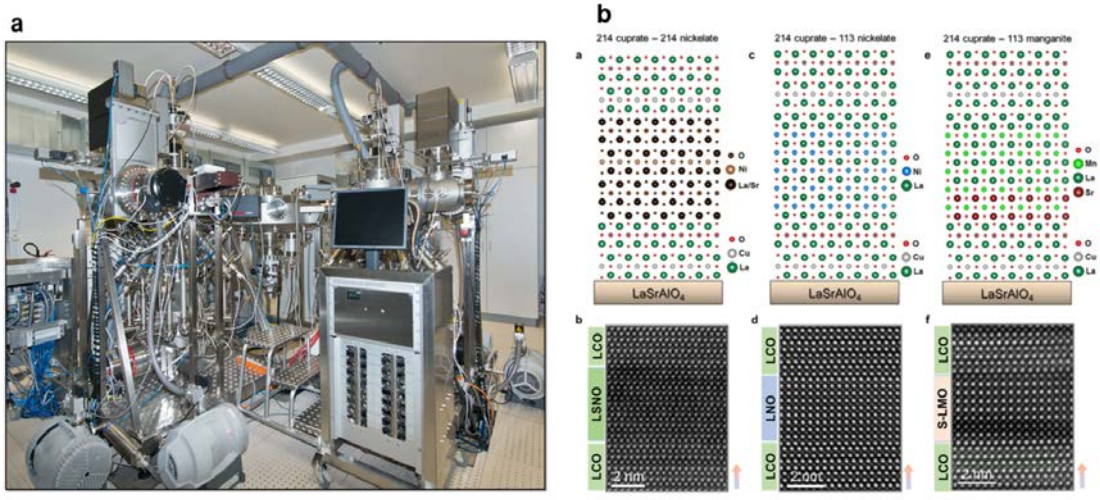

Figure 8. Atomic-layer precise oxide MBE (a) and aberration-corrected STEM of oxide structures (b). from [7]

The relevance of "functionable" interface designs can not be emphasized enough. Besides the need for atomic-level characterization techniques, engineering concepts for the generation of complex oxide heterostructures have to be put in place. Atomically precise deposition technologies, such as oxide molecular beam epitaxy have dramatically improved the quality of such interfaces, and in a review paper within ESTEEM3 WP7 ICT, **recommendations are given on how deposition parameters impact interfacial qualities**. [7]

Another studied phenomenon was the electromechanical coupling between strain gradients and **polarization**, giving rise to "**flexoelectricity**" in an epitaxial system of $SrMnO_3/SrTiO_3$, featuring cracks that are known to generate largest strain gradients at the tip of the cracks (figure 8). Through a combination of **HAADF STEM imaging, geometric phase analysis** and by analyzing **atomic displacements**, the polarization could be calculated from the displacement between the position of the Ti atom and the centroid of the neighbouring Sr columns. Accompanied by unusual electronic and chemical states present at crack tips, shown with **EELS**, this finding implies that flexoelectricity may influence the processes of crack formation and propagation considerably. [8]

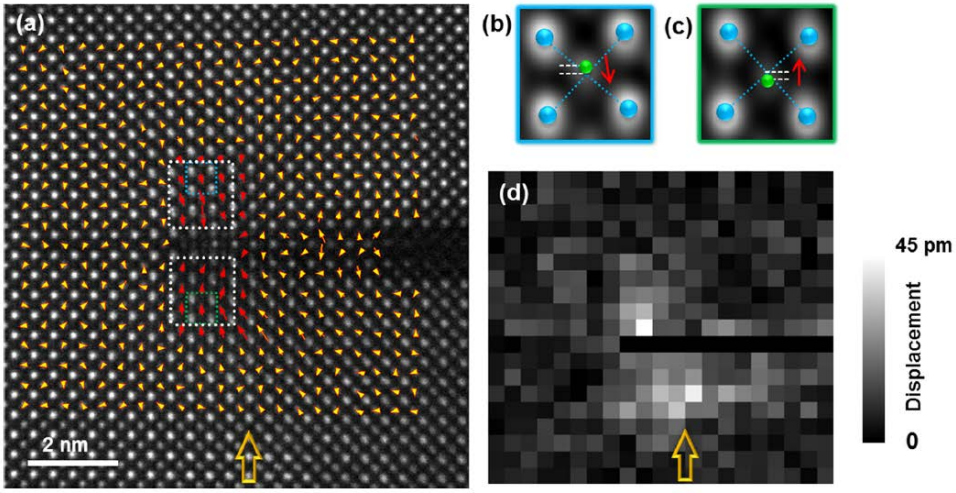

Figure 9. Lattice displacement analysis around the deep crack. (a) Displacement vector map between the TiO and Sr columns overlaid with the HAADF image. Polarization is observed in a region about 3–4 unit cells surrounding the crack tip (red arrows). (b, c) Schematic images for the relative displacement of TiO columns with respect to the four neighboring Sr columns. (d) Magnitude map of displacement vectors in the region defined by the red and yellow arrows in part a. from [8]

In a ferroelectric field-effect device (here a combination of a ferroelectric $BiFeO_3$ and a doped Mott insulator $Ca_{0.96}Ce_{0.04}MnO_3$), **polarization switching** at the micron scale by **piezo response force microscopy was correlated with HAADF STEM-EELS** observations on cross-sectioned specimens. Fundamental information on polarization switching phenomena at interfaces and their influence on the electronic properties of the adjacent layer could be obtained. The real space and spectroscopic observations at the atomic scale indicate that the "switched" regions actually consist of heterogeneous configurations with various fractions of upwards/downwards polarization domains in the volume of the ferroelectric. Nanoregions with switched interfacial polarization **generate large variations of the carrier concentrations** in the adjacent manganite layer, consistently with the large polarization of $BiFeO_3$. These results hold promises for the practical developments of ferroelectric field-effect transistors and other non-volatile low power devices.

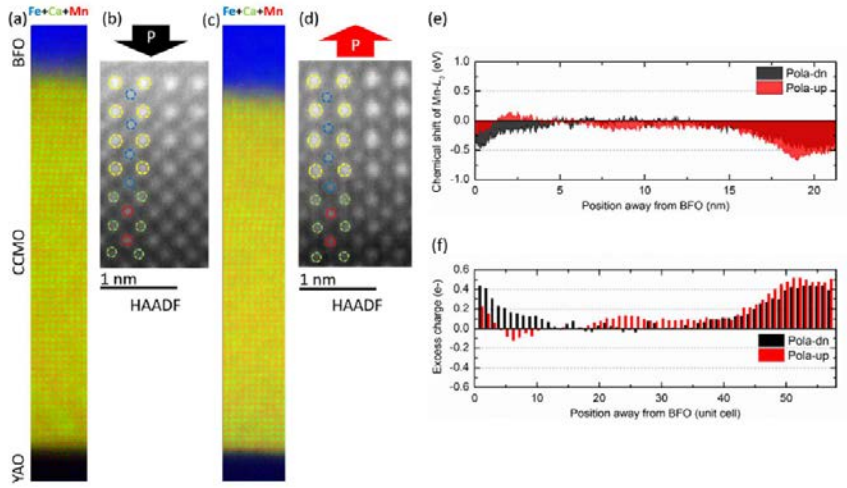

Figure 10. Polarization switching in a ferroelectric field-effect device, from [9]

It must be noted that the complexity of physical effects related to electronic changes and structural modifications inevitably requires method combinations, like in the example above, which extend the core topic of this TEM-centered project. **Polarized x-ray absorption spectroscopy (XAS)** or confocal **Raman spectroscopy** for instance were shown to serve as sensitive probes of the electronic and vibrational properties of vacancies, which can dramatically alter the resistivities and superconductive behavior of the $SrRuO_3$ system. Ruthenium vacancies showed different Raman signatures in metallic and superconducting samples, and in ruthenium deficient SRO, the O *K*-edge XAS exhibited a considerable suppression of the spectral weight in the pre-peak structures stemming from Ru-O hybridization. It is hence the correlation of different characterization modalities that augment our understanding in terms of a structure property relationship. [9]

Another functionality of complex oxides for ICT derives from the high ion mobility of oxygen-deficient thin film oxides, which might be in non-volatile memories based on resistive switching or solid oxide fuel cells. This phenomena is based on the onset of local physico-chemical transformations induced by the application of electric fields and currents, which drives oxygen migration. In this case, we have studied by aberration corrected HAADF-STEM the topotactic transformation induced in $SrFeO_{3-\delta}$ films by the local application of electric fields with an AFM tip [10]. This work has evidenced that epitaxial $SrFeO_{3-\delta}$ films, which present a conducting perovskite-type structure with randomly oriented vacancies, transforms into an insulating brownmillerite $SrFeO_{2.5}$ phase. Furthermore, the as-grown state can be restored upon annealing in oxygen atmosphere. $SrFeO_{3-\delta}$ in perovskite phase is unusually unstable in comparison with other perovskite-based structures, and sophisticated cryo-FIB procedures have been followed to guarantee that the as-grown and transformed phases are conserved during TEM lamella preparation. Future work will be devoted to analyzing in detail the atomic structure of both phases, and attempting the study of the transformation kinetics by in-situ biasing inside the TEM. [10]

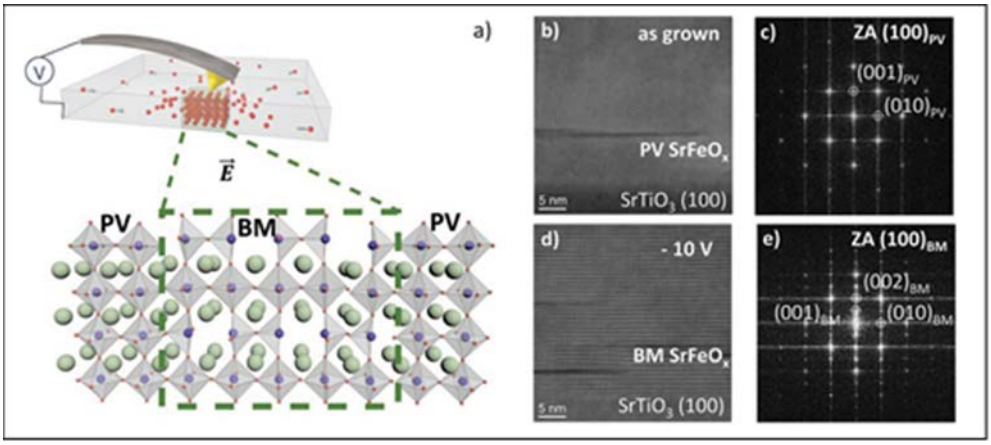

Figure 11. (AFM electric-field-induced local topotactic transformation. a) Applying an electrical voltage between the AFM tip and the PV $SrFeO_{3-\delta}$ film in contact mode produces a large electric field in the region underneath the tip (b-e) (b) and (c) show the STEM and Fourier transform of a pristine area of the film, showing the microstructure of the PV film. Panels (d) and (e) show the same microstructural analysis of a lamella extracted from an region scanned at −10 V, showing the characteristic morphology and superstructure spots of the BM phase. from [10]

Within this task 1D and 2D hybrid materials have also been studied, and work is ongoing. An example on novel misfit layered compounds (MLC) in the form of nanotubes shall exemplify preliminarily the power of **TEM based characterization techniques correlated with external modalities.** The present results show that the structural, **plasmonic, and vibrational properties** of the $Y_xLa_{1-x}S$-TaS_2 MLC can be tuned by variation of the Y content, making them highly interesting for applications, e.g., for **plasmon technology in the IR range**. TEM analyses (HR(S)TEM, EDS, EELS and diffraction) revealed the structure and chemical composition of this NTs. This is crucial for having information about the growth of such nanostructures and then improving their synthesis, as well as for understanding their properties. [11]

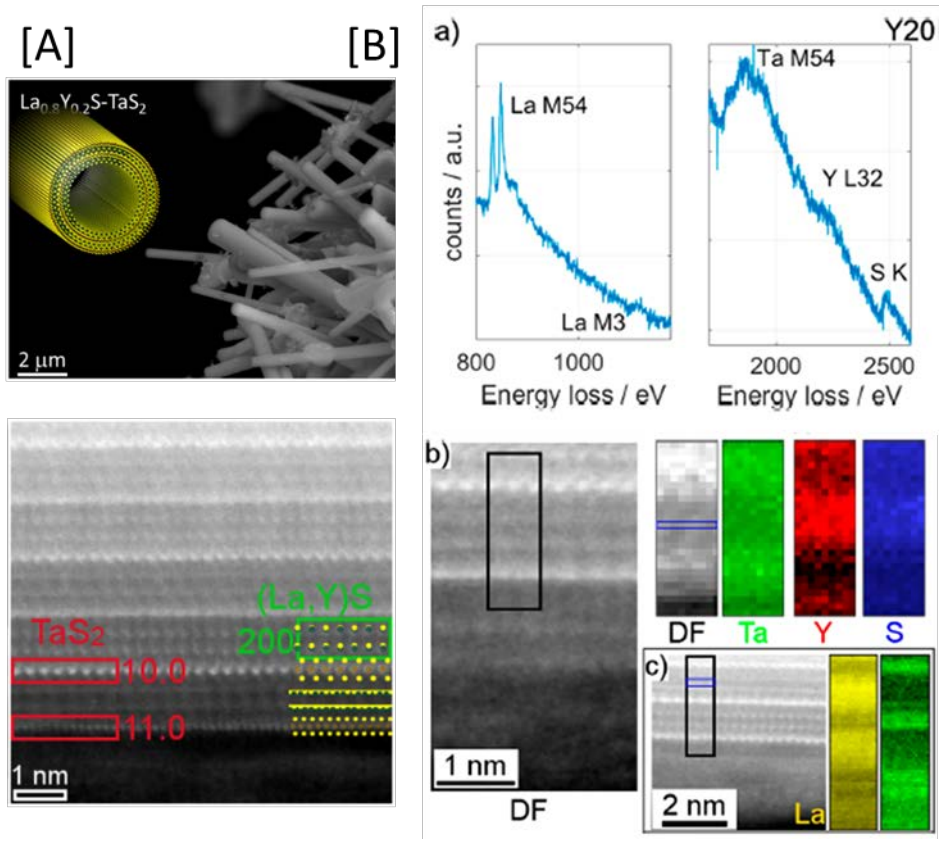

Figure 12. Nanotubes based on misfit layered compounds: $Y_xLa_{1-x}S$-TaS_2 ($0 \leq x \leq 1$) family. [A] Top: Schematic representation of a (Y,La)S-TaS_2 NT formed by two layers of the stack with the b-axis coinciding with the tube axis. SEM micrographs of the tubular structures. Bottom: HAADF-STEM image of a NT from a sample containing 20% of Y. The appearance of the layer stack alternates along the c-axis, revealing two folding vectors rotated by 30° with respect to each other. Identified projections of the different layers are marked in green and red for the (La,Y)S and the TaS_2 subunits, respectively. [B] (a) EELS analysis of an NT from sample Y20. (a) Spectra of the La M-edge as well as the Ta M-, Y L-, and S K-edges are taken from regions marked blue in the dark field (DF) images in b and c, respectively. (b) Ta and Y are spatially separated between the different layers recognized in the DF image. (c) La spectrum image obtained on the same NT showing enrichment of La in the two layers of MS. from [11]

It is anticipated that several other techniques, worked on in different WPs, or the employment of differential phase contrast imaging to study electric and magnetic field effects will enter this work package in due course. This is in synchronization with the development and best use principles elaborated in other packages like WP 4,5,6.

Task 7.3: Photonic materials (GRA, ZAR, STU, ORS, CHA)

The characterization of photonic materials and the understanding of the manifold phenomena found in nano-optics through TEM and related methods is a highly dynamic branch in this work package, manifested by the number of different systems, physical effects and potential applications - an overview shall be given.

Phonons, i.e lattice vibrations in solids, determine some of the fundamental properties in solids, and their localization on surfaces have recently attracted a lot attention due to promising applications in nanophotonics. Unlike surface plasmons they offer excellent quality factors, yet to understand their potential for technology, a thorough three-dimensional understanding of the electro-magnetic field is necessary. With recent **STEM-EELS** instruments, approaching **sub-10meV energy resolution** and innovative reconstruction algorithms, the **3D electromagnetic local density of states** has become accessible (manuscript in preparation) and can now be tackled for other complex systems.

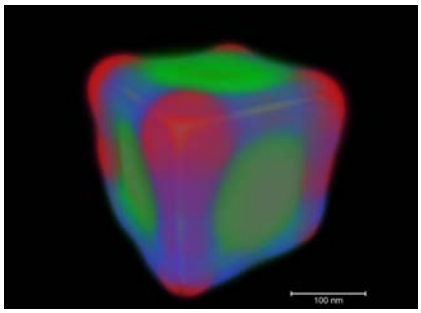

Figure 13. 3D reconstruction of different phonon modes in MgO.

In the presence of a plasmon local field, phonons get strongly modified and, in particular, their dipolar strengths are highly enhanced. This modification of vibrational modes in nanostructures could be monitored by **high-energy resolution EELS** measurements by a **tailored coupling of plasmon resonances in metallic Ag nanowires to phonon modes in h-BN thin flakes**. Using electron-beam controlled milling, the energies of the plasmon modes could be continuously shifted to resonate with specific h-BN vibrational modes, and thereby new effects such as strong coupling between surface phonons and surface plasmons; enhancement of the bulk vibrational EELS signal; and the emergence of geometry-forbidden dark phonon modes could be found. [12]

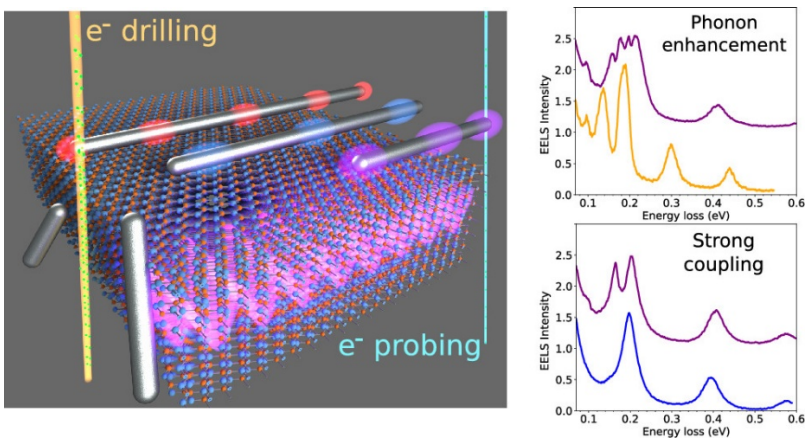

Figure 14. (left) Silver nanowires deposited on h-BN. (right) Spectral changes upon coupling. from [12]

P**lasmon** responses have been studied also on complex material systems beyond pure metals, such as **sodium tungsten bronze nanocubes**; the optical properties of which are tunable with stoichiometry. Depending on the cube sizes, local Na-depletion, explored by **energy-dispersive X-ray spectroscopy** (EDXS), had different impact, as confirmed by Boundary Element Method **(MNPBEM toolbox) simulations** (manuscript in preparation).

The role of **EDXS** shall be emphasized further by showing results from a **magnetically doped topological insulator** such as **Mn-doped Bi_2Te_3**. Tetradymite structures are three dimensionally strong topological insulators with realistically large (a few hundred meV) bulk gaps and simple surface electronic structures. The tetradymite lattice, with its van der Waals gap between the quintuple layers, provides however many different electrically and magnetically inequivalent incorporation sites. The site-specific incorporation of the Mn dopant atoms is key for understanding their impact on magnetism and topology of the system and this intricate interplay between topological order and ferromagnetism inspired a few proposals to realize exotic quantum phenomena, such as the magnetoelectric effect and quantum anomalous Hall effect. Unexpectedly, upon growth of the system, a self-organizing stacking sequence consisting of additional sextuple layers (SL; universal for other systems like Bi_2Se_3 and isovalent dopants) has formed. With **Mn located interstitially** in the middle of the SL rather than substitutionally in the lattice, the common notion of dopant incorporation in former studies has to be revisited.[13]

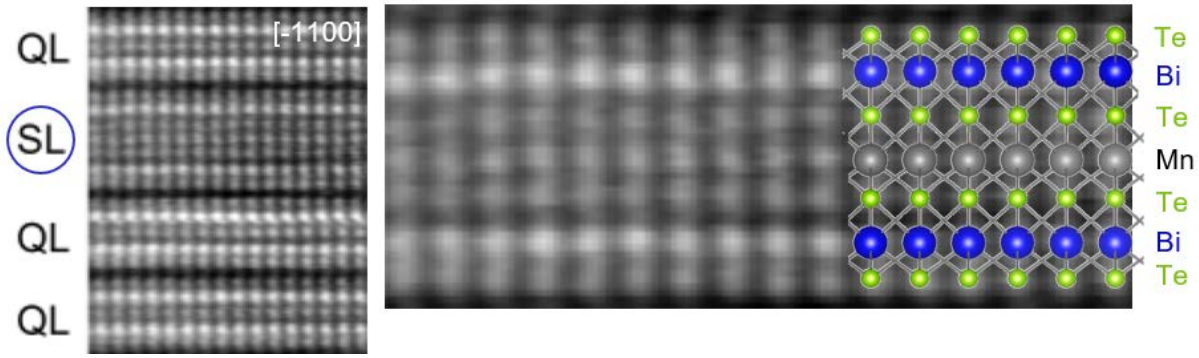

Figure 15. Magnetically doped topological insulator Mn: Bi_2Te_3. from [13]

An interesting example for an application of **plasmonic nanostructures in photo catalysis** is based on anisotropic, prisms and triangular-shaped Au-ZnO photocatalysts, grown onto ZnO nanoparticles. The combination of experimental **EELS** measurements (**in combination with HAADF**) and **Finite-Difference-Time-Domain (FDTD)** theoretical calculations suggest a strong interaction at the interface between metal and semiconductor. The LED-driven photooxidation of n-hexane has revealed an enhanced response upon irradiation with the more energetic wavelengths, suggesting a **predominant role of intraband electrons** from the metallic nanostructures. The results show a promising candidate for multiple photocatalytic reactions of interest in environmental and energy applications. [14]

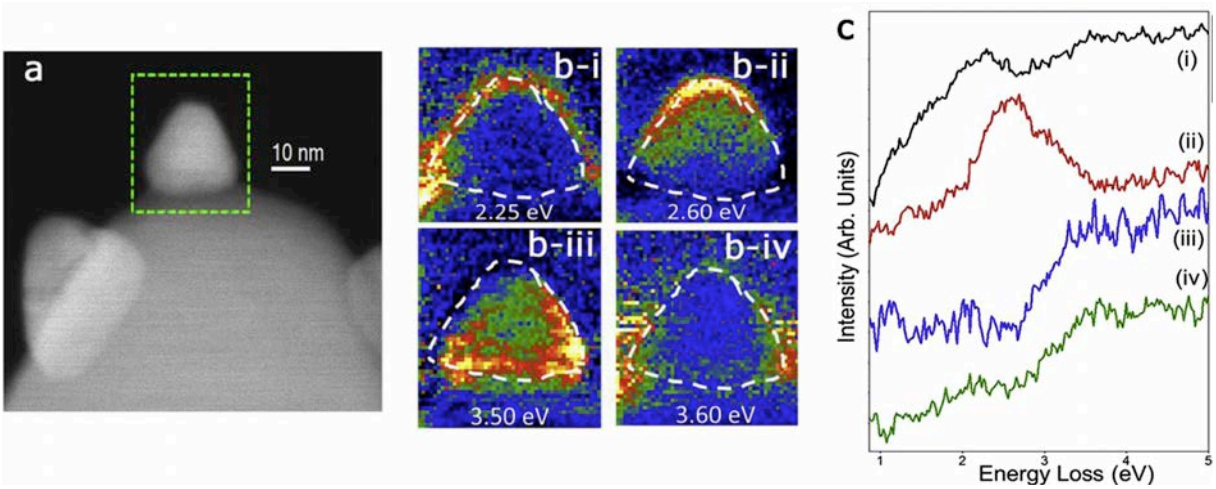

Figure 16. HAADF-STEM and EELS plasmon maps of a Au-ZnO nano photo-catalytic system. from [14]

Nanoscale **polaritons** (light-matter quasiparticles) are important across many disciplines due to their hybrid half-light half-matter character. Strong light-matter coupling has received significant attention across various scientific fields, including recent progress in light-matter coupling in 2D materials, observation of Bose-Einstein condensation of polaritons, photon blockade, and new emerging field of "polaritonic chemistry". In this work package, polaritons have been visualized with unprecedented spatial resolution and unexpected nanometer-scale variations and their properties have been shown. Specifically, electron energy loss spectroscopy in scanning transmission electron microscope has been used to visualize strong coupling and nanoscale vacuum Rabi splitting in a plasmon-exciton hybrid nanostructure consisting of individual silver nanoparticle coupled to a few-layer transition metal dichalcogenide WS_2 flake. The work establishes **EELS as an essential characterization tool for studying plexcitons**. This technique has very clear advantages in terms of insights to the coupled system and capabilities that no other characterization technique can offer, including: sensitivity to absorption signal instead of scattering signal, correlation between optical microscopy and EELS signal originating from the very same plexcitonic nanostructure and deep nanoscale-resolved coupling strength and detuning. **STEM EELS provides clear insights on the very existence of plexcitons and about their inner nature**. [15]

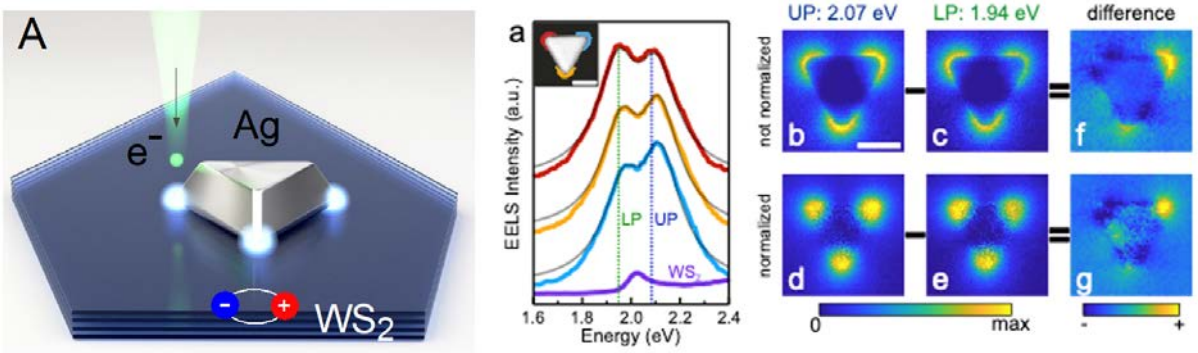

Figure 17. (A) Plasmon-exciton hybrid system, exciting a strongly coupled plexciton system composed of a Ag TNP and few-layer WS_2. (a) Spatially and spectrally resolved variations of plexcitons and (b-g) EELS maps of the coupled system. from [15]

Relativistic electron beams are known to create optical radiation when interacting with tailored nanostructures, leading to a potentially **new appliance**. An artificial **mesoscopic structure**, composed of an array of nanoscale holes in a gold film, acting as a lens, was designed using transformation optics to deliver ultrashort chirped electromagnetic wave packets upon 30–200 keV electron irradiation. In contrast to diffractive metamaterial-based planar lenses, the proposed element sustains an ultra-broadband spectral feature both in the near- and far-field and maintains its focusing ability for all spectral components. The design principle offers large tunability in controlling both illumination angle and focal length and due to the plasmon-induced mechanism of radiation, it acts as a **coherent electron-driven photon source**. Femtosecond photon bunches result from coherent scattering of surface plasmon polaritons with hyperbolic dispersion. They decay by radiation in a broad spectral band which is focused into a 1.5 micrometer beam waist at 5.7 µm distance from the structure. The focusing ability and broadband nature of this photon source will initiate applications in ultrafast spectral interferometry techniques. **A combination of methods such as energy-filtering TEM, angle-resolved cathodoluminescence and time-dependent simulations have enabled this result.** [16] Other structures such as three-dimensional plasmonic gold tapers have also been studied with regard to their radiation properties in the proximity of the apex. [17]

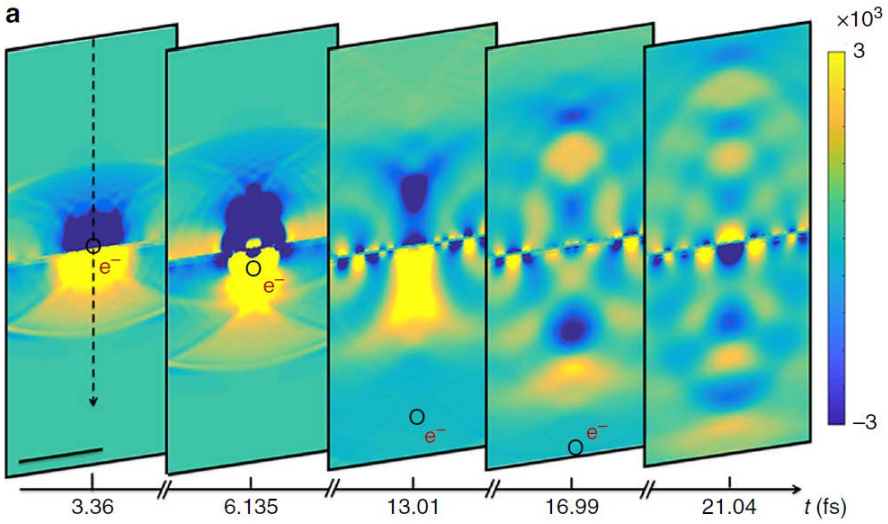

Figure 18. Simulated spatio-temporal response of the planar lens interacting with a 30 keV electron. (a) Snapshots of the z-component of the electric field amplitude at depicted times for the indicated electron positions. from [17]

Beyond the well-known elementary electromagnetic sources (moments), such as linear electric and magnetic multipoles, **toroidal multipoles** are considered as another family of elementary EM sources due to their distinct charge-current configuration and unique parity properties. Techniques such as **cathodo-luminescence, EELS and STEM** have turned out as powerful combinations to elucidate fundamental questions related to those moments such as optical activity and electromagnetic-induced transparency. **Focused ion beam milling** allows for an efficient generation of metallic nanocavities to study their radiation behaviours. [18, 19]

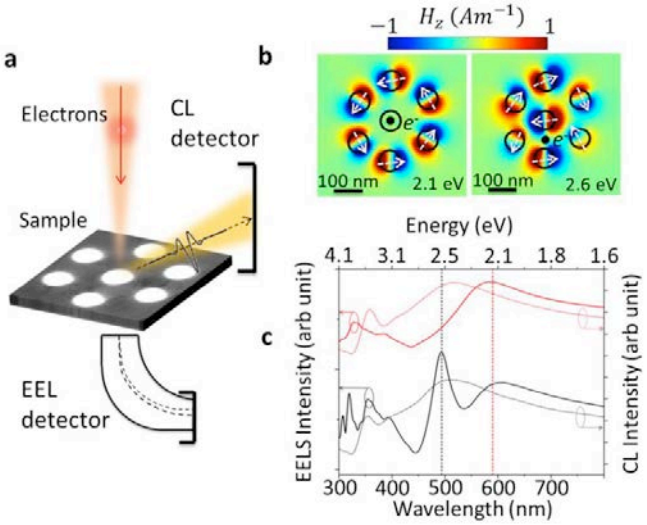

Figure 19. The hexamer nanocavity structure is excited by focused electron probes in a TEM, and the scattered electrons and photons are both detected using electron energy-loss and cathodoluminescence spectroscopy. from [18]

Task 7.4: Sample preparation (GRA, ZAR, STU, CHA, TOU*, CAT*)

In ICT characterization, a few specimen preparation techniques have turned out to be particularly useful. Unless for powder or particle type of samples, the criteria for the selection of a suitable technique have boiled down to: quality i.e. avoidance of preparation artifacts, site specifity, micromanipulation, nanostructuring and speed.

Avoidance of preparation artifacts:

The lengthiest, yet least invasive technique is wedge polishing. Micrometers adjustment screws allow for a precise sample tilt adjustment relative to an abrasive plane. Speed rotation and oscillation can be varied to maximize use of the entire grinding/polishing disc and to minimize artifacts. In addition, adjustable load control enable the handling delicate samples. Parallel polishing, angle polishing and -with some restrictions- site-specific polishing can be achieved. Practically, the combination of wedge polishing with a final low-energy ion milling step under cryo conditions has yielded the most arti-fact free specimens with the least amount of amorphous cover layers. Wedge polishing with subsequent post milling is clearly recommended and was mostly used for brittle and delicate systems such as in tasks 1 and task 2. To spread expertise, various trainings and exchange activites have taken place within the consortium, for instance between GRA and STU.

Site-specifity, micromanipulation, nanostructuring and speed:

In terms of throughput and site-targeting, focused ion beam instruments (FIB) essentially have no alternatives. Cross-sections of bottom-up structures (semiconductor devices, substrate grown films etc.) can be generated within 2-4 hours for typical specimen areas. Attention has to be paid to the respective milling parameters, and already within the ESTEEM2 project, optimized milling protocols have been created, which are continuously updated. It is absolutely key to set up low beam currents and acceleration voltages for the final optimization step, ideally under cryo-cooling conditions. For this, either dedicated instruments need to be used (NanoMill by Fischione) or the build-in FIB optics already

allows for it by itself. FIBS often feature micro manipulation devices that are essential to connect and pick up nano-structures for selective analysis, for instance when handling nano-wires. Also their structuring capabilities by either removal of material (for the generation of lenses, shortening of nano-wires etc.) or by deposition of materials (FEBID) is essential for ICT materials. Again training programs between GRA, STU and ZAR are in place and help disseminating the specific knowledge for best operation of these instruments.

On a side note it shall be mentioned that electro-chemical etching, applicable mostly to metallic systems, has proven to be a powerful alternative to quickly generate needle-type samples, suitable for 3D tomographic investigations. (A respective instrument is available to serve other WPs i.e WP10). This ought to be explored further for other potentially suitable material systems.

Summary

In summary and as shown, crystal imperfections and atomic-scale defects permit tailoring material properties into the diverse combinations that modern engineering devices require, defining electronic and optical properties of innovative photonic and semiconducting materials. It´s fair to state that direct imaging methods like high-angle annular dark-field imaging and annular bright-field imaging, so far have proven to be most helpful for the characterization of ICT materials. Their capability to visualize material contrast on an atomic scale, allowing for a direct derivation of the crystallographic structure, including defects, is of utmost importance to the understanding of the fundamental physics but also of their potential applications in technology. In this respect and for this work package, they have excelled over reciprocal space techniques, which have been applied to a minor amount only. It is foreseeable that throughout the course of this project, holography and differential phase contrast microscopies will have further impact on the findings in this work package.

Added value comes in through spectroscopic techniques such as cathodo-luminescence, X-ray and electron energy-loss spectroscopies that link together structural, electronic and chemical information. Other non-TEM based techniques such as Raman, IR, AFM / MFM, RIXS etc. have shown significant importance to this work package also, yet a closer correlation of the respective analysis scales and better integration into the overall analysis process is desirable and needs to be tackled.

EELS has proven to be of extreme relevance, and its capability to deliver spatially, atomically resolved (or momentum) information at the level of phonon losses makes it rather unique. The linkage to CL and vibrational spectroscopies is still in its infancies but offers great potential. It has to be emphasized that today, aberration-corrected, high energy-resolution STEM EELS represents one of the most powerful characterization tools available for ICT studies.

References (selected papers only)

[1] “In situ real-time annealing of ultrathin vertical Fe nanowires grown by focused electron beam induced deposition”. Javier Pablo-Navarro, Robert Winkler, Georg Haberfehlner, Cesar Magen, Harald Plank and Jose María De Teresa. **Acta Materialia 174 (2019) 379 – 386**

[2] “Customized MFM probes based on magnetic nanorods”. Miriam Jaafar, Javier Pablo-Navarro, Eider Berganza, Pablo Ares, César Magén, Aurélien Masseboeuf, Christophe Gatel, Etienne Snoeck, Julio Gómez-Herrero, José María de Teresa and Agustina Asenjo. **Nanoscale 12 (2020) 10090**

[3] “Exotic Transverse-Vortex Magnetic Configurations in CoNi Nanowires”. Ingrid Andersen, Luis Alfredo Rodríguez González, Cristina Bran, Cécile Marcelot, Sébastien Joulié, Teresa Hungría, Manuel Vazquez, Christophe Gatel and Etienne Snoeck. **https://hal.archives-ouvertes.fr/hal-02406354**

[4] “The impact of swift electrons on the segregation of Ni-Au nanoalloys”. Daniel Knez, Martin Schnedlitz, Maximilian Lasserus, Andreas W. Hauser, Wolfgang E. Ernst, Ferdinand Hofer and Gerald Kothleitner. **Appl. Phys. Lett. 115 (2019) 123103**

[5] “The Effect of Bending Deformation on Charge Transport and Electron Effective Mass of p-doped GaAs Nanowires”. Lunjie Zeng, Thomas Kanne, Jesper Nygård, Peter Krogstrup, Wolfgang Jäger and Eva Olsson. **Phys. Status Solidi RRL 13 (2019) 1900134**

[6] “High-temperature-grown buffer layer boosts electron mobility in epitaxial La doped $BaSnO_3/SrZrO_3$ heterostructures”. Arnaud P. Nono Tchiomo, Wolfgang Braun, Bryan P. Doyle, Wilfried Sigle, Peter van Aken , Jochen Mannhart and Prosper Ngabonziza. **APL Mater. 7 (2019) 041119**

[7] “Design of Complex Oxide Interfaces by Oxide Molecular Beam Epitaxy”. Y. E. Suyolcu, G. Christiani, P. A. van Aken and G. Logvenov. **J Supercond. Nov. Magn. 33 (2020) 107–120**

[8] “Direct Observation of Huge Flexoelectric Polarization around Crack Tips”. Hongguang Wang, Xijie Jiang, Yi Wang, Robert W. Stark, Peter A. van Aken, Jochen Mannhart and Hans Boschker. **Nano Lett. 20 (2020) 88–94**

[9] “In-depth atomic mapping of polarization switching in a ferroelectric field-effect transistor”. Xiaoyan Li, Qiuxiang Zhu, Lorenzo Vistoli, Agnès Barthélémy, Manuel Bibes, Stéphane Fusil, Vincent Garcia2 and Alexandre Gloter. **DOI:10.1002/admi.202000601**

[10] “Room-Temperature AFM Electric-Field-Induced Topotactic Transformation between Perovskite and Brownmillerite $SrFeO_x$ with Sub-Micrometer Spatial Resolution”. Elías Ferreiro-Vila, Santiago Blanco-Canosa, Irene Lucas del Pozo, Hari Babu Vasili, César Magén, Alfonso Ibarra, Juan Rubio-Zuazo, Germán R. Castro, Luis Morellón, Francisco Rivadulla. **Advanced Functional Materials 29 (2019) 1901984**.

[11] “YS-TaS_2 and $Y_xLa_{1-x}S$-TaS_2 ($0 \le x \le 1$) Nanotubes: A Family of Misfit Layered Compounds”. Simon Hettler, M. B. Sreedhara, Marco Serra, Sudarson S. Sinha, Ronit Popovitz-Biro, Iddo Pinkas, Andrey N. Enyashin, Reshef Tenne and Raul Arenal. **ACS Nano 14 (5) (2020) 5445-5458**

[12] “Tailored Nanoscale Plasmon-Enhanced Vibrational Electron Spectroscopy”. Luiz H. G. Tizei, Vahagn Mkhitaryan, Hugo Lourenço-Martins, Leonardo Scarabelli, Kenji Watanabe, Takashi Taniguchi, Marcel Tencé, Jean-Denis Blazit, Xiaoyan Li, Alexandre Gloter, Alberto Zobelli, Franz-Philipp Schmidt, Luis M. Liz-Marzán, F. Javier García de Abajo, Odile Stéphan and Mathieu Kociak. **Nano Lett. 20 (2020) 2973–2979**

[13] “Large magnetic gap at the Dirac point in $Bi_2Te_3/MnBi_2Te_4$ heterostructures”. E. D. L. Rienks, S. Wimmer, J. Sánchez-Barriga, O. Caha, P. S. Mandal, J. Růžička, A. Ney, H. Steiner, V. V. Volobuev, H. Groiss, M. Albu, G. Kothleitner, J. Michalička, S. A. Khan, J. Minár, H. Ebert, G. Bauer, F. Freyse, A. Varykhalov, O. Rader and G. Springholz. **Nature 576 (2019) 423**

[14] “Anisotropic Au-ZnO photocatalyst for the visible-light expanded oxidation of n-hexane”. Carlos J. Bueno-Alejo, Javier Grausa, Raul Arenal, Marta Lafuente, Bruno Bottega-Pergher and Jose L. Hueso. **Catalysis Today (2020) https://doi.org/10.1016/j.cattod.2020.03.063**

[15] “Visualizing Spatial Variations of Plasmon−Exciton Polaritons at the Nanoscale Using Electron Microscopy”. Andrew B. Yankovich, Battulga Munkhbat, Denis G. Baranov, Jorge Cuadra, Erik Olsén, Hugo Lourenço-Martins, Luiz H. G. Tizei, Mathieu Kociak, Eva Olsson and Timur Shegai. **Nano Lett. 19 (2020) 8171−8181**

[16] “Merging transformation optics with electron-driven photon sources”. Nahid Talebi, Sophie Meuret Surong Guo, Mario Hentschel, Albert Polman, Harald Giessen and Peter A. van Aken. **Nat Commun 10 (2019) 599**

[17] “Far-Field Radiation of Three-Dimensional Plasmonic Gold Tapers near Apexes”. Surong Guo, Nahid Talebi, Alfredo Campos, Wilfried Sigle, Martin Esmann, Simon F. Becker, Christoph Lienau, Mathieu Kociak and Peter A. van Aken. **ACS Photonics 6 (2019) 2509−2516**

[18] “Toroidal Moments Probed by Electron Beams”. Nahid Talebi, Surong Guo, Alfredo Campos, Mathieu Kociak and Peter A. van Aken. **J. Phys.: Conf. Ser. 1461 (2020) 012174**

[19] “Radiation of Dynamic Toroidal Moments”. Surong Guo, Nahid Talebi, Alfredo Campos, Mathieu Kociak and Peter A. van Aken. **ACS Photonics 6 (2019) 467−474**